Article

Not peer-reviewed version

A Hybrid Photo-Catalytic Approach Utilizing Oleic Acid-Capped ZnO Nanoparticles for the Treatment of Wastewater Containing Reactive Dyes

Zakia H. Alhashem , Ashraf H Farha * , Shrouq H. Aleithan , Shehab A. Mansour , Maha A. Tony

Posted Date: 14 October 2024

doi: 10.20944/preprints202410.1039.v1

Keywords: Advanced catalysis; Fenton; Hybrid; Oxidation; ZnO-Oleic acid; Thermodynamics

Article

A Hybrid Photo-Catalytic Approach Utilizing Oleic Acid-Capped ZnO Nanoparticles for the Treatment of Wastewater Containing Reactive Dyes

Zakia H. Alhashem [1], Ashraf H. Farha [1,2,*], Shrouq H. Aleithan [1], Shehab A. Mansour [1,3,4] and Maha A. Tony [3,4]

[1] Department of Physics, College of Science, King Faisal University, Al-Ahsa 31982, Saudi Arabia
[2] Semiconductors Technology Lab, Physics Department, Faculty of Science, Ain Shams University, Cairo 11566, Egypt
[3] Advanced Materials/Solar Energy and Environmental Sustainability (AMSEES) Laboratory, Faculty of Engineering, Menoufia University, Shebin El-Kom 32511, Egypt
[4] Basic Engineering Science Department, Faculty of Engineering, Menoufia University, Shebin El-Kom 32511, Egypt
* Correspondence: afarha@kfu.edu.sa

Abstract: In pursuit of overcoming Fenton's oxidation limitations in wastewater treatment, an introduction of heterogeneous photocatalyst is developed. In this regard, the current work is introducing ZnO nanocrystals that were successfully prepared by thermal decomposition technique and then capped with oleic acid (OA). The synthesized ZnO-OA and the pristine ZnO were characterized by X-ray diffraction (XRD), Fourier transform infrared spectroscopy (FTIR) and field emission scanning electron microscopy (FE-SEM). Then, the study introduces the application of such materials in advanced oxidation processes, i.e. Fenton's reaction to treat dye-containing wastewater. Synthetic wastewater that prepared using Reactive Blue 4 (RB4) is used as a simulated textile wastewater effluent. Fenton's oxidation is applied, and the system parameters were assessed using the modified Fenton's system. The synthesized samples of ZnO are characterized by a recognized wurtzite hexagonal structure. Modifying the surface of ZnO with oleic acid (OA) led to an increase in crystallite size, lattice parameters, and cell volume. These modifications are linked to the efficient capping of ZnO nanoparticles by OA, which further improved the dispersion of the nanoparticles, as demonstrated by SEM imaging. The optimum conditions of ZnO and ZnO-OA synthesized modified Fenton composites showed 400, 40 mg/L for H_2O_2 and catalyst respectively, at pH 3.0 within 90 min under UV irradiation for maximal dye oxidation reached 93%. The catalytic performance at its optimal circumstances was in accordance with a pseudo-second-order kinetics model for both ZnO-OA and the pristine ZnO based Fenton's systems. Also, the thermodynamic parameters were also checked and the values settled that both Fenton systems are spontaneous in nature, proceeds at a low energy barrier condition (10.38 and 31.38 kJ/mol for ZnO-OA and the pristine ZnO based Fenton reaction, respectively).

Keywords: Advanced catalysis; Fenton; Hybrid; oxidation; ZnO-Oleic acid; thermodynamics

1. Introduction

No doubt the production of textiles and textile industries are playing a significant role in the economics of countries all around the world [1]. Countries that signified as the leading exporters in this field are China, the European Union, India, USA, Korea, Turkey and Pakistan [2]. The textile industry could be such dry or wet manufacturing processes. The dry process involves separation of fibers from the sources, spinning and weaving into clothes [3,4]. However, through the wet operating system, textiles are reacted step-wise with chemicals and rinsed using water. Thus, wet processing consumes massive amounts of fresh water that could be 200 L/kg of textile as well as a high load of

 doi:10.20944/preprints202410.1039.v1

organic and inorganic substances [5–7]. Synthetic dyes are extensively used in this industry to attain a bright and firm color for textiles [2,3]. Such material is categorized as organic compounds that possess a complex aromatic molecular structure [8]. On the other hand, the presence of such complex aromatic molecular structures in those dyes makes them very stable, have a high toxic impact, color and challenges them to be biodegradable [9–11]. Thus, despite the importance of such textile industrial activity, the release of such dyes in the discharge of the textile effluent is considered a critical environmental issue [8,12,13]. Accordingly, massive environmental deterioration and toxic upsets to humans have arisen [14].

Numerous types of commercial textile dyes are produced and applied in the textile industry all over the globe [15–17]. However, reactive dyes represent nearly 12% of worldwide manufacturing [18]. Extensive application of such reactive dyes is detected in the textile industry because of the tendency of their reactive groups to produce covalent bonds that support fixing such substance color into the fabrics [19,20]. Consequently, the interaction between the fabrics and the dye substance is enhanced and, thereby, overall energy consumption in the technique is less [2,21–23]. However, their utilization in practical application is still a concern since their toxic discharge into the industry [6,24]. In this regard, treating the textile discharge effluents is a must for both ecosystem conservation and human and aquatic creatures' protection [25–27].

Currently, great efforts have been applied to dealing with and treating such discharge to substitute the conventional methodologies [28]. Commonly for long decades, adsorption [29], flocculation [30], and filtration [31] were applied to treat such discharges. But such systems are unfavorable since they are non-destructive by transporting the contaminant from phase to another without destroying one [32]. Consequently, the result is a secondary pollutant that needs further treatment [33]. In this regard, scientists' interest is searching for advanced systems for so-called advanced oxidation processes (AOPs). AOPs are gaining great significance since they are eco-friendly techniques, since their end products are CO_2 and H_2O [17,34]. Such systems are based on the generation of in situ hydroxyl (•OH) radicals attacking the pollutant molecules and destroying them. Fenton's reagent among such AOP techniques is signified as an efficient method since its •OH radicals' yield is high [35,36]. In such a reaction, H_2O_2 is induced Fe^{2+} in an acidic medium to produce the radicals, and the oxidation is undertaken through a successive reaction. However, the traditional homogeneous Fenton reaction is unfavorable since the iron catalyst is easily deactivated due to iron-based systems, weak Fenton activity in the ultraviolet range from iron leaching, and the final iron sludge presence after treatment. Thus, to overcome such inherent shortcomings, a solid heterogeneous Fenton-based catalyst is essential to upgrading the Fenton system. Transition metal oxide semiconductors are seen as viable possibilities. Among these, ZnO's unique qualities, such as its wide band gap, high chemical stability, non-toxicity, and ease of synthesis, have led to a surge in its use as an environmental photocatalyst in the photodegradation of contaminants [31]. Despite this, there are several drawbacks to using ZnO as a photocatalyst, such as the high possibility of photoinduced electron-hole recombination. In this regard, numerous studies have been conducted to enhance the separation rate of photoinduced charge carriers by altering the electronic energy band structure of photocatalysts through doping with metallic ions [37]. Our prior investigation on ZnO surface modification with oleic acid (OA) resulted in a blue shift in the optical band gap and increased Urbach tails at the margins of the valence and conduction bands by 64.3 and 80.4 meV, respectively [38]. These variations in the energy band layout with increasing trap site density may improve the photocatalysis efficiency of ZnO by reducing the recombination process between photoinduced electrons and holes.

The current work investigates the effect of capping ZnO nanocrystals with OA on the UV degradation of Reactive Blue 4 (RB4) organic dye. The pure ZnO nanocrystals were manufactured using the thermal decomposition approach, which is an excellent low-cost and high-yield method after calcinations of zinc acetate salt, given its low decomposition temperature [39]. Afterwards, the prepared materials are applied to oxidize the RB4 dye. The reaction operational parameters including initial dye load, hydrogen peroxide and catalyst concentrations as well as the operating pH are

 doi:10.20944/preprints202410.1039.v1

studied. Also, the thermodynamic parameters are assessed and the reaction kinetic model is investigated.

2. Materials and Methods:

2.1. Synthesis of ZnO Nanocrystals

ZnO nanocrystals have been synthesized by utilizing a simple thermal decomposition method. This standard preparation approach has been documented elsewhere [39]. Zinc acetate dihydrate ($Zn(CH_3COO)_2{\cdot}2H_2O$; Winlab, purity: 99.999%) has been utilized as the precursor in the synthesis of ZnO nanocrystals. Approximately 15 g of $Zn(CH_3COO)_2{\cdot}2H_2O$ was placed in a covered 50 mL alumina crucible and subjected to a decomposition procedure in an oven at 350 °C for 3.5 hours. The chosen heating settings were employed to guarantee the complete thermal decomposition of the precursors [38,40].

2.2. Capping ZnO Nanocrystals with Oleic Acid (OA)

Oleic acid [$C_{18}H_{34}O_2$, OA, Alfa Aesar] was utilized to cap and modify the surface of the ZnO nanocrystals as they were manufactured. The approach to surface modification was described elsewhere [41,42]. In the conventional technique, 1 g of ZnO nanocrystals, 60 mL of water, and 3 mL of OA are added to a beaker, and the mixture is ultrasonicated for 30 minutes. After that, the mixture was agitated for 8 hours using a magnetic stirrer. Following the reaction, the liquid was centrifuged for one hour. To wash, add 60 mL of ethanol to the precipitate and expose to ultrasonic for 30 minutes. The resulting solution will be centrifuged for one hour. The final two steps were repeated three times. The resulting precipitate is dried under vacuum at room temperature to provide the final product, ZnO-OA. Figure 1 depicts the schematic design for the capping of as-synthesized ZnO nanocrystals with oleic acid.

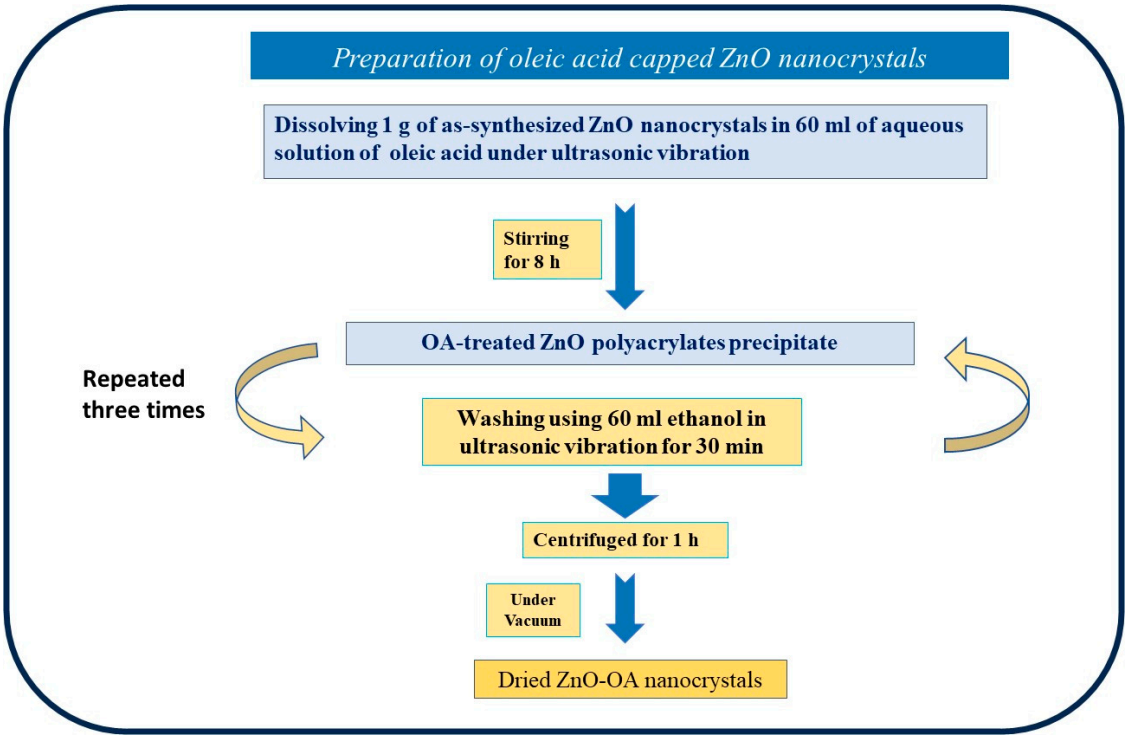

Figure 1. Schematic diagram for the capping of as-synthesized ZnO nanocrystals with oleic acid.

2.3. Bench Scale Set-Up

1-Amino-4-[3-(4,6-dichlorotriazin-2-ylamino)-4-sulfophenylamino] anthraquinone-2-sulfonic acid, which is so-called Reactive Blue 4 (RB4) dye was used as a model pollutant. An accurately

 doi:10.20944/preprints202410.1039.v1

weighed quantity of such powder was dissolved in distilled water to prepare 1000-ppm of stock dye solution that was further diluted to the required value. Diluted H_2SO_4 and NaOH are used to adjust the pH, when desired, to the required values. All chemicals are used as received with no further purification.

Experiments of chemical oxidation reaction were carried out in a lab-scale batch mode as shown in the graphical representation of the treatment steps (Figure 2). Initially, the pH of the wastewater was adjusted to the required values if needed. 100 mL of aliquot Reactive Blue 4 (RB4) dye as the contaminating wastewater with the desired concentration were subjected to a catalytic oxidation reaction through a magnetic stirring and the reaction was initiated by the hydrogen peroxide addition. Then, an artificial UV light source provided by a high intensity 254 nm (UV-A, 70W/m^2 lamp) was applied to the wastewater sample. Afterwards, samples were checked periodically for spectrophotometric analysis.

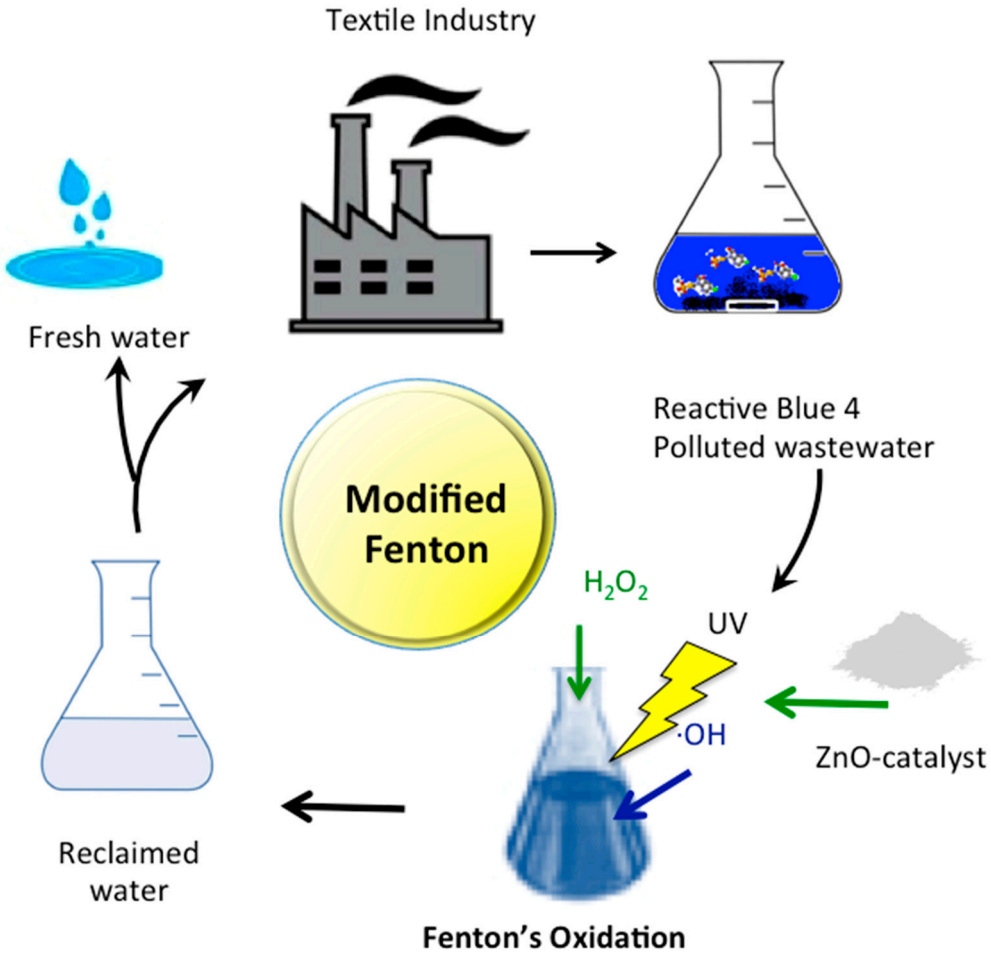

Figure 2. Graphical representation of the treatment steps and experimental set-up.

2.4. Analytical Determination

The wastewater concentration before and after treatment technique was evaluated by its spectrophotometric analysis using spectrophotometer (UV–visible spectrophotometer, model Unico UV-2100 spectrophotometer, USA). The pH of the wastewater samples it was monitored using a digital pH-meter model AD1030, Adwa instrument (Hungary).

2.5. Characterization Techniques for as-Synthesized ZnO and ZnO-OA Nanocrystals

The phase structure of ZnO and ZnO-OA was investigated using an X-ray diffractometer (XRPhillips X'pert, MPD 3040) equipped with a monochromatic CuKa source (λ = 0.15406 nm). To analyze X-ray diffraction (XRD), diffracted intensities were collected from 10 to 80° using a step-scan

 doi:10.20944/preprints202410.1039.v1

mode with 0.02° steps. The FTIR transmittance spectra of the materials were obtained using a JASCO (FT/IR-4100) spectrometer over the wave number 400 to 4000 cm^{-1}. The morphology of ZnO and ZnO-OA nanocrystals was studied with a Quanta FEJ20 field-emission scanning electron microscope (FE-SEM).

3. Results and Discussions

3.1. Structural and Morphological Characterization of as-Synthesized ZnO and OA-ZnO

XRD results for both ZnO and ZnO-OA samples are illustrated in Figure 3. The phase identification and XRD data refinement were performed using the Rietveld analysis through theFullProf software (FullProf Suite 5.10), amid the resulting parameters illustrated in Figure 3. The XRD peaks of the ZnO sample are accurately aligned with the ZnO wurtzite hexagonal structure standard data (space group: P 63 m c). The absence of additional peaks in ZnO sample confirms nonexistence of any other phase. It is important to highlight that, the lattice parameters a and c according to the identified phase are showing increasing from 3.2513 and 5.2085 Å to 3.2524 and 5.2112 Å, for ZnO and ZnO-OA samples, respectively. These are resulting in an increase in the unit cell volume of from 47.681$Å^3$ to 47.741 ZnO and ZnO-OA samples, respectively as shown in Table 1. Both samples exhibit a strong texture in [101] direction, as shown in Figure 3. The XRD peaks are significantly lowered in ZnO-OA sample compared to as-synthesized ZnO sample. This drop in peak intensity imitate a decrease in crystallinity of ZnO-OA sample comparative to as-synthesized one. There are some strong XRD peaks in lower 2θ (10-30°) as well as an amorphous hump that appeared only in the ZnO-OA pattern, which are attributed to modification of the surface of ZnO by oleic acid.

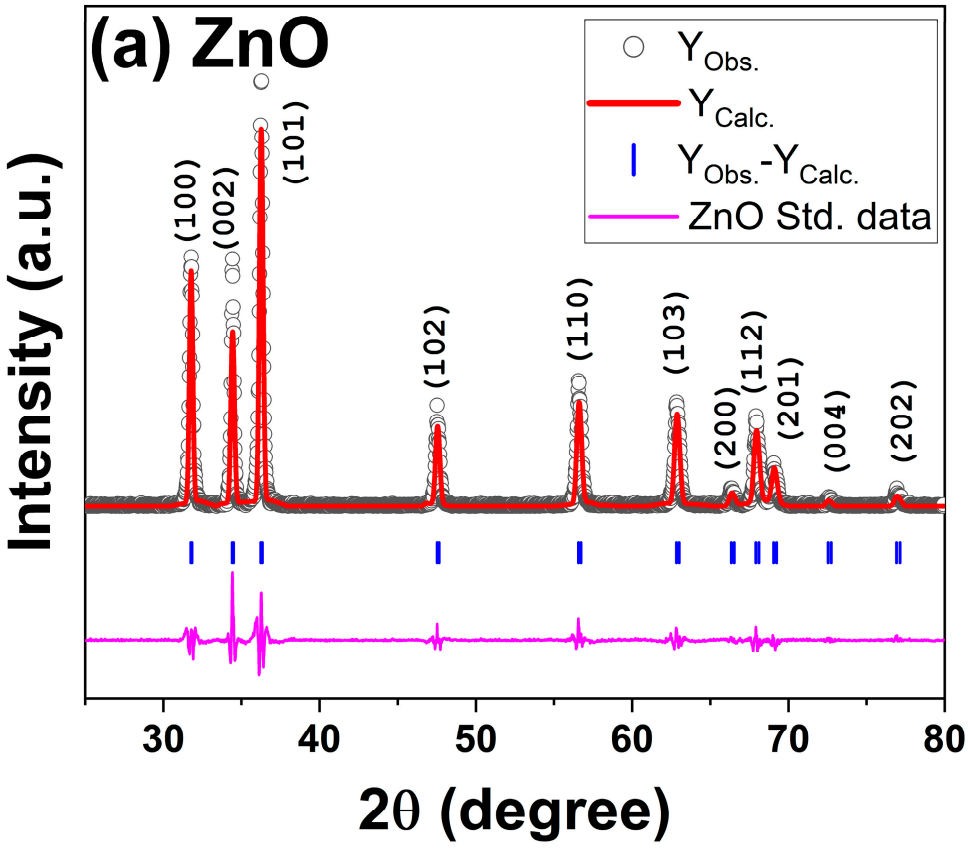

 doi:10.20944/preprints202410.1039.v1

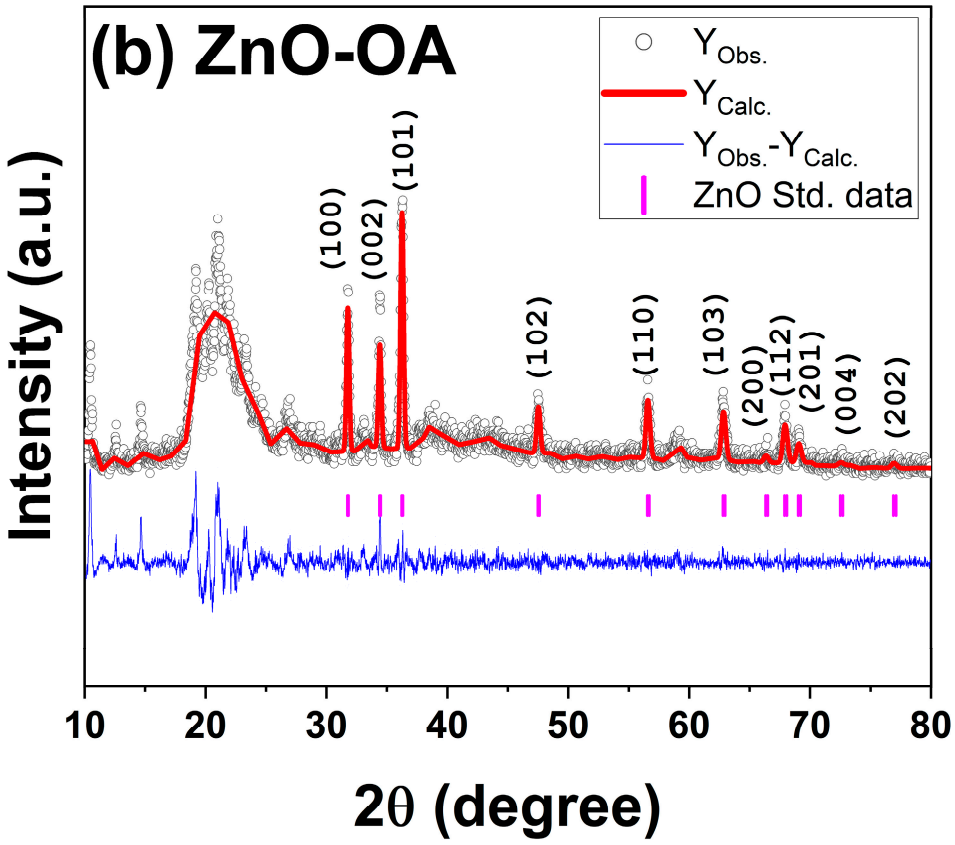

Figure 3. XRD patterns with Rietveld analysis according to ZnO standard data for (a) ZnO and (b) ZnO-OA samples.

The average crystallite size and induced microstrain of both samples were determined from the Williamson–Hall plot [43]. The Williamson-Hall plot is shown in Figure 4 ($4\sin\theta$ vs. $\beta\cos\theta$) of ZnO and ZnO-OA, where β is FWHM of XRD peaks and θ is the Bragg`s diffraction angle. The average crystallite size value increses from 43.3 nm to 46.2 nm for ZnO and ZnO-OA, respectively. The Williamson–Hall analysis also yielded an increase in the induced microstrain from 0.0008 to 0.0012 for ZnO and ZnO-OA samples. It demonstrates that ZnO-OA has broader peaks than ZnO sample, which has sharper and more peaks. As a result, surface modification by OA leads to such change [38,42].

Table 1. The average crystallites size, microstrain (ε), the lattice constants (a & c) and the cell volume ZnO and ZnO-OA samples.

	Crystallite Size, nm	Microstrain (ε)	a, Å	c, Å	Cell Volume, (Å)$^{-3}$
ZnO	43.3	0.0008	3.2513	5.2085	47.681
ZnO-OA	46.2	0.0012	3.2524	5.2112	47.741

Preprints.org (www.preprints.org) | NOT PEER-REVIEWED | Posted: 14 October 2024 doi:10.20944/preprints202410.1039.v1

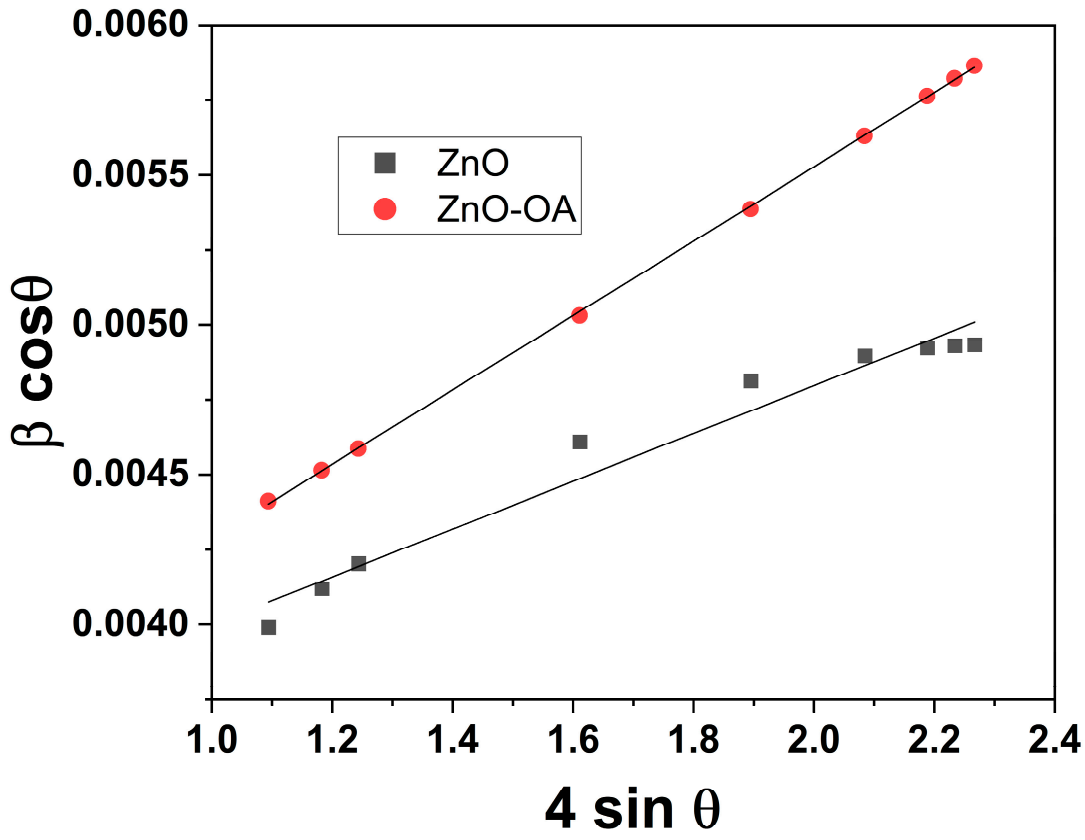

Figure 4. The Williamson-Hall plot ($4sin\theta$ vs. $\beta\cos\theta$) of ZnO and ZnO-OA samples.

Fourier Transform Infrared (FTIR) spectroscopy was used to thoroughly evaluate the impact of oleic acid (OA) surface treatment on ZnO. The FTIR transmittance bands for both ZnO and ZnO-OA samples are listed in Table 2. The FTIR results show a wide band in low wave number range due to Zn and O stretch within ZnO. The produced ZnO and ZnO-OA exhibit absorption bands around 407 and 406 cm^{-1}. The vibration modes at 1536 cm^{-1} and 1654 cm^{-1} in ZnO and 1543 cm^{-1} and 1700 cm^{-1} indicate asymmetric and symmetric stretching of C=O, respectively. While the absorption band at 3417 cm^{-1} and 3417 cm^{-1} are corresponding to O-H stretching vibration from zinc acetate in ZnO and ZnO-OA, respectively.

one noting that the oleic acid molecules surrounding the ZnO nanoparticles causes an enhancement in the absorption bands of ZnO-OA sample in contrast to ZnO sample. This suggests that the treatment with oleic acid aids in achieving a well-dispersed configuration of ZnO nanoparticles. The FTIR of ZnO-OA show a variety of notable absorption bands that are characteristic of free oleic acid. Significant features include the asymmetric and symmetric stretching modes of $-CH_2$ groups of the oleic acid hydrocarbon chain, which are appearing at 2851 and 2920 cm^{-1}, respectively. Additionally, the C=O stretch vibration at 1396-1456 cm^{-1} and 1526 cm^{-1}, due to symmetric and asymmetric carboxylate stretch of oleate. Which are important highlights to the presence of the carboxylic acid functional group within the oleic acid molecule. of course The emergence of all these OA-related peaks clearly confirms that the surface fictionalization of ZnO nanoparticles has been successfully accomplished [38,42,44].

 doi:10.20944/preprints202410.1039.v1

Table 2. The FTIR transmittance bands for both ZnO and ZnO-OA samples.

Functional Group	Wave number (cm^{-1})	
	ZnO	ZnO-OA
Zn–O stretch	407	406
	663	683
C=O stretch	1536	1543
	1654	1700
–CH_2 stretch	–	2851
	–	2920
carboxylate stretch (oleate)	–	1396–1456
	–	1526
O–H stretch (acetate)	3407	3417

To analyze the microstructure and morphology of ZnO and ZnO-OA nanocrystals, FE-SEM equipment was utilized. It is for this reason that the micrographs of these modified nanocrystals are displayed in Figure 5. The shape of the synthesized zinc oxide that was achieved is a nanorod shape with aggregation zones appearing in a flower-like pattern, as shown in Figure 5a,b. For the thermal decomposition process of ZnO, it is frequently reported that the synthesized ZnO forms nanorods, which are a one-dimensional (1D) nanostructure shape [39]. In fact, the avoidance of the addition of chemical ligands is responsible for the production of 1D-ZnO that is anticipated to occur in this method of synthesis. In most cases, the utilization of chemical ligands results in the regulation of crystal formation in a specific crystallographic direction [40]. On the other hand Figure 5c,d, serve illustrations of the creation of capped ZnO nanorods using OA.

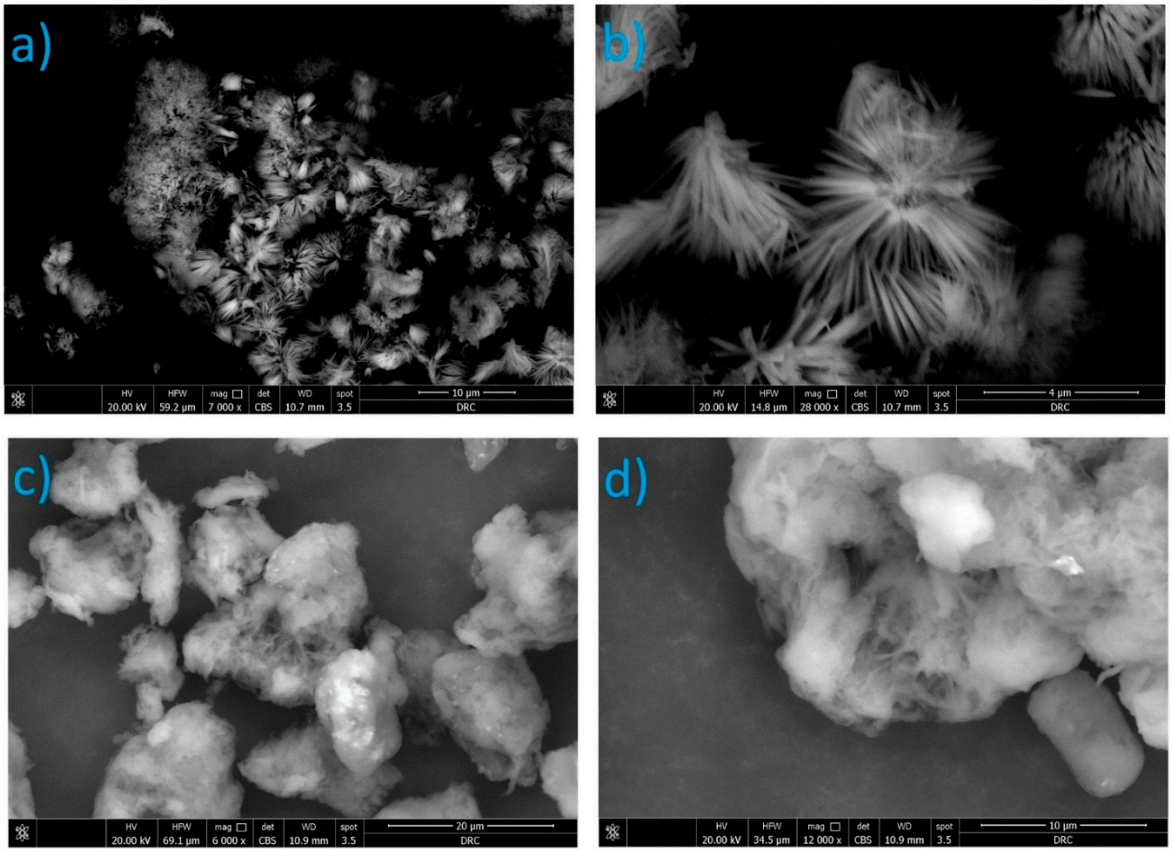

 doi:10.20944/preprints202410.1039.v1

Figure 5. FE-SEM micrographs of the synthesized ZnO nanocrystals: (a) 7,000× magnification and 10 μm scale; (b) 10,000× magnification and 4 μm scale and ZnO-OA nanocrystals: (c) 6,000× magnification and 20 μm scale; (d) 12,000× magnification and 10 μm scale.

3.2. Studies on RB4 Dye Oxidation

3.2.1. RB4 Dye Oxidation Related to Contact Time between Different Oxidation Systems

Initially, in order to design the oxidation matrix, it is essential to monitor the illumination time. The time-profile of RB4 dye oxidation using pristine ZnO and capped ZnO with OA in dark and UV illumination as well as their Fenton system were studied at room temperature and displayed in Figure 6. The data presented in Figure 6 shows a comparison of the RB4 dye removal effectiveness as a function of reaction time with the various systems at room temperature and pH 3.0. It is clear that both ZnO and ZnO-OA systems under the UV illumination based modified Fenton systems were effective on dye removal. Overall, the highest removal rate is achieved when ZnO-OA /H_2O_2/UV is applied after 90 minutes of illumination time.

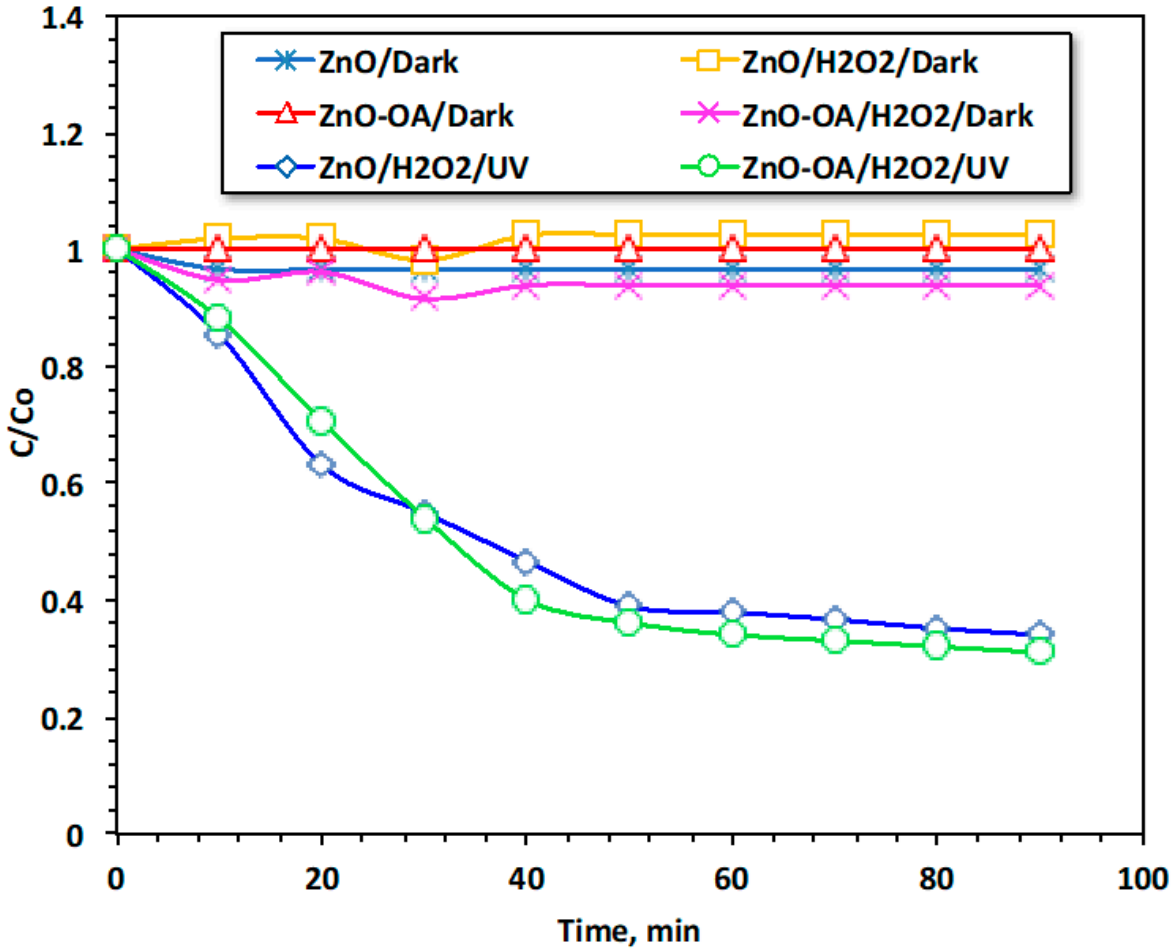

Figure 6. Effect of reaction time on different oxidation systems.

Interestingly, no recognized dye oxidation is achieved for the solo ZnO system or ZnO-OA. Furthermore, the Fenton-based systems in the dark also results in no dye oxidation compared to a high removal compared to the other UV-illumination systems. This confirms the role of the ZnO and ZnO-OA as a Fenton system. This oxidation rate for the modified Fenton oxidation systems is associated to the •OH radicals generated. However, such radicals gradually declined with exceeding of time, corresponding to the reduction in the H_2O_2 concentration with the formation of other radicals, which inhibit the reaction rate rather than increasing the RB4 dye oxidation [45–47].

 doi:10.20944/preprints202410.1039.v1

Also, in the Fenton system, the oxidation system arises by exploiting the activation of H_2O_2 with semiconductor salt for highly reactive hydroxyl radical (•OH) generation. However, such hydrogen peroxide is consumed after the initial reaction period. Subsequently, a complex reaction happens and such reaction generates extra radicals that is named hydroperoxyl radicals (HO_2). The oxidation reaction is influenced by both hydroxyl and hydroperoxyl radicals. Nevertheless, HO_2 radicals possess a lower oxidation capability in comparison to the •OH radicals. Accordingly, the RB4 dye oxidation rate is deduced with time proceeding. Numerous studies [48–51]. have shown the oxidation rate is quicker in the initial reaction time since the immediate creation of the •OH radicals.

3.2.2. Effect of Initial RB4 Loading on Oxidation System

On the textile indusial wastewater discharge basis, the pollutant loading in aqueous streams is discharged on a varied daily basis. Hence, in this regard, it is urgent to assess Fenton's oxidation dependence on the RB4 dye loading. Consequently, RB4 dye loading is varied from 5 to 40 ppm to evaluate the modified Fenton's oxidation efficiency by increasing the RB4 dye concentration, whereas all other experimental parameters that influence the Fenton's reaction are kept at its optimum values (pH 3.0; hydrogen peroxide 400 and catalyst 40 mg/L, respectively).

The data exhibited in Figure 7a,b are the average of three replicates designating that load of the RB4 dye concentration, resulting in a reduction in its oxidation efficacy reaching 55 and 57% when the RB4 dye concentration was 40 ppm for ZnO and ZnO-OA based Fenton's systems, respectively. But the removal increased to 94% and complete removal (100%) when the RB4 dye loading is low at 5 ppm for ZnO and ZnO-OA based on Fenton's systems, respectively. This might be associated with the short lifetime of •OH radicals' species, which is signified as the controller of the Fenton's oxidation system. Oxidation is improved through improving the tendency of collision between the radical species and RB4 dye molecules in the wastewater system. Hence, the result is enhancing the rate of RB4 dye oxidation. However, the increase in the RB4 dye load is leading to a reduction in Fenton's oxidation efficacy. This is due to the number of active sites of the ZnO supporting Fenton's system reaction is inadequate for the too high RB4 dye concentration. Furthermore, the high concentration of RB4 dye in the aqueous stream results in a reduction in the light absorption through the hydrogen peroxide that is required for the Fenton system under UV-illumination, so reduced the hydroxyl radical species.

It is noteworthy to mention that extra time is essential to reach the required treatment efficiency. Further, treating higher RB4 dye loading at the same catalysts and reagent concentrations, it could not reach a higher removal rate. This trend of reducing the oxidation rate by increasing the initial pollutant concentration in the aqueous stream was previously recorded by several researchers [38,52,53] in treating different types of wastewaters with Fenton's system.

 doi:10.20944/preprints202410.1039.v1

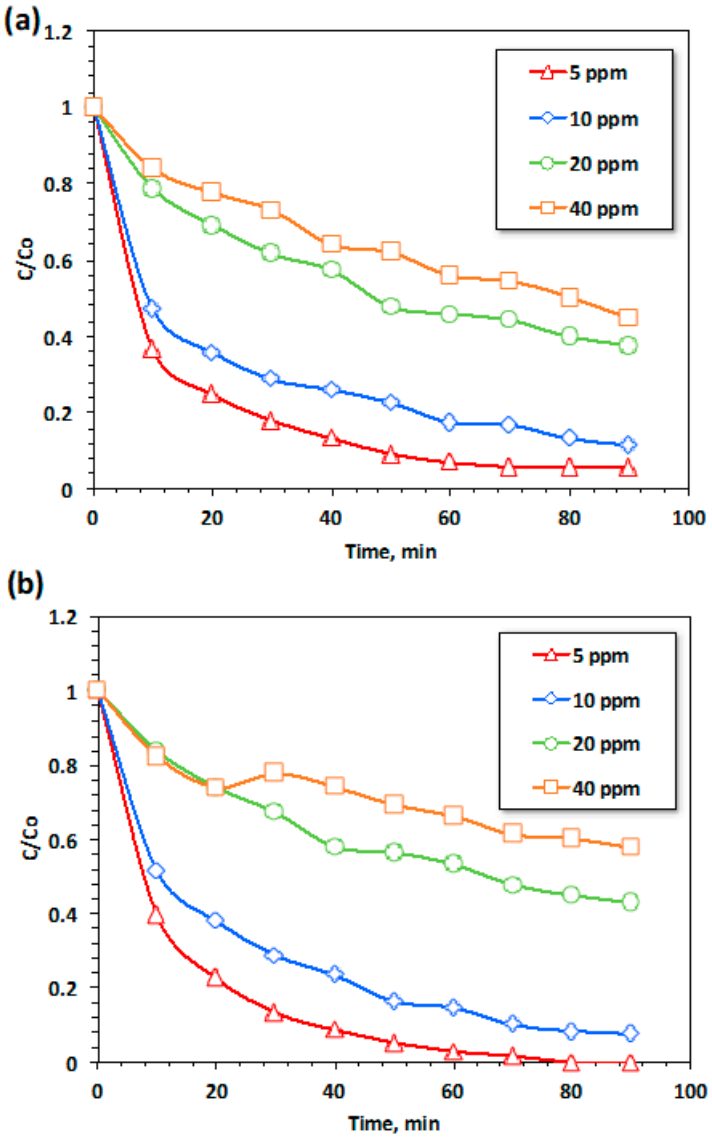

Figure 7. The Effect of RB4 dye loading on the oxidation rate (operating conditions at pH 3.0; H_2O_2 400 mg/L and catalyst 40 mg/L) for (a) ZnO and (b) ZnO-OA based Fenton`s systems.

3.2.3. The Effect of Different Fenton Parameters on Oxidation Behavior

3.2.3.1. Effect of ZnO and ZnO-OA Dosing

In order to evaluate the effect of ZnO and ZnO-OA doses on the RB4 dye removal rate, the catalyst concentration was added in the reaction medium from 20 to 80 mg/ L, whereas the other parameters were kept constant (hydrogen peroxide dose was kept constant at 400 mg/L and the initial pH at 3.0). It is displayed in Figure 8a,b using ZnO and ZnO-OA, respectively. The results displayed in Figure 8 revealed that for both systems ZnO and ZnO-OA, increasing the catalyst dose results in an elevation in the rate of RB4 dye oxidation and the maximal rate reached, 88 and 93% when 40 mg/L is added for ZnO and ZnO-OA based Fenton's systems, respectively. But, further catalyst dose addition of extra than 40 mg/L exposed a reduction in the removal of RB4 dye to 67 and 73% with the catalyst addition of 80 mg/L, for ZnO and ZnO-OA based Fenton's systems, respectively.

Interestingly, adverse effects of extra catalyst concentration on the solution were attained since the excess addition of the catalyst speciation in the aqueous medium hinders the •OH radicals' performance. This could be illustrated by the •OH radicals being trapped by excess catalyst ions. Hence, 40 mg/L is signified as the optimum concentration needed for RB4 ye oxidation in both the

 doi:10.20944/preprints202410.1039.v1

modified ZnO and ZnO-OA based Fenton's systems. Similar results were revealed in treating dye contaminated effluent by modified Fenton system that highlighted the extra excess catalyst dose that hinders the Fenton's system [52]. Also, the ZnO-OA based Fenton's system showed a higher oxidation rate reaching 93%, which confirms the modified ZnO catalyst is superior to the ZnO without capping with oleic acid. Such results verify the well capping interface of OA on ZnO nanoparticles [45].

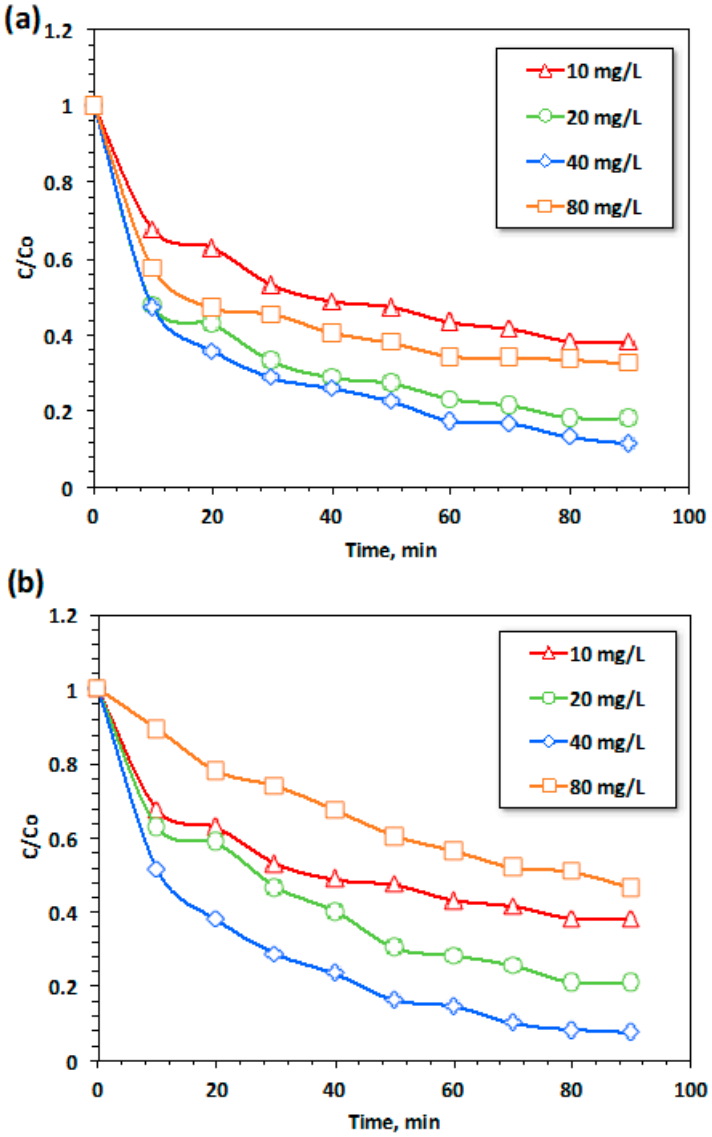

Figure 8. The effect of catalyst concentration on RB4 oxidation at pH 3.0 and H_2O_2 400 mg/L for (a) ZnO and (b) ZnO-OA based Fenton's systems.

3.2.3.2. Effect of Hydrogen Peroxide

Hydrogen peroxide is categorized as a significant factor to improve and induce the hydroxyl radical's generation in the Fenton media. For producing hydroxyl radicals in the Fenton's reaction, it is essential to decompose H_2O_2 in the presence of the catalyst, i.e. ZnO. Furthermore, it is crucial to maintain both H_2O_2 or catalyst concentrations minimum whereas their excess concentrations deduce the reaction proficiency. Hence, to test the effect of H_2O_2 on the Fenton's oxidation of RB4 dye, experiments were carried out to assess the effect of hydrogen peroxide concentration on the reaction rate.

 doi:10.20944/preprints202410.1039.v1

Figure 9a,b exhibited the effective RB4 dye oxidation by varying H_2O_2 concentrations within the range of 100 to 800 mg/L. The oxidation efficacy improved from 45% to 88% when the hydrogen peroxide concentration increases from 100 to 400 mg/L, respectively for the ZnO based Fenton system (Figure 9a). While the corresponding dye removals reached to 46 and 93%, respectively for the ZnO-OA based Fenton system (Figure 9b). Furthermore, for both systems further H_2O_2 increase more than extra than 400 mg/L, results in a diminution in RB4 dye removal efficacy that decreases to 73% when 800 mg/L is applied for H_2O_2 reagent. Nevertheless, a further reduction in the oxidation efficiency with the upsurge in hydrogen peroxide dose was achieved. This might be attributed by the excess H_2O_2 in the reaction medium, more than the optimal dose; H_2O_2 itself would performances as $^{\bullet}OH$ scavenger rather than a producer and result is creating HO_2 radicals. Such HO_2 radicals' species are minimal reactive when comparable with $^{\bullet}OH$ radicals and thereby a negligible contribution is attained. Additionally, the produced HO_2 radicals in the system medium react with the remaining $^{\bullet}OH$ radicals. This examination was previously reported by the different researcher [35]. Thus, the result is a terminal effect in the RB4 dye oxidation efficiency.

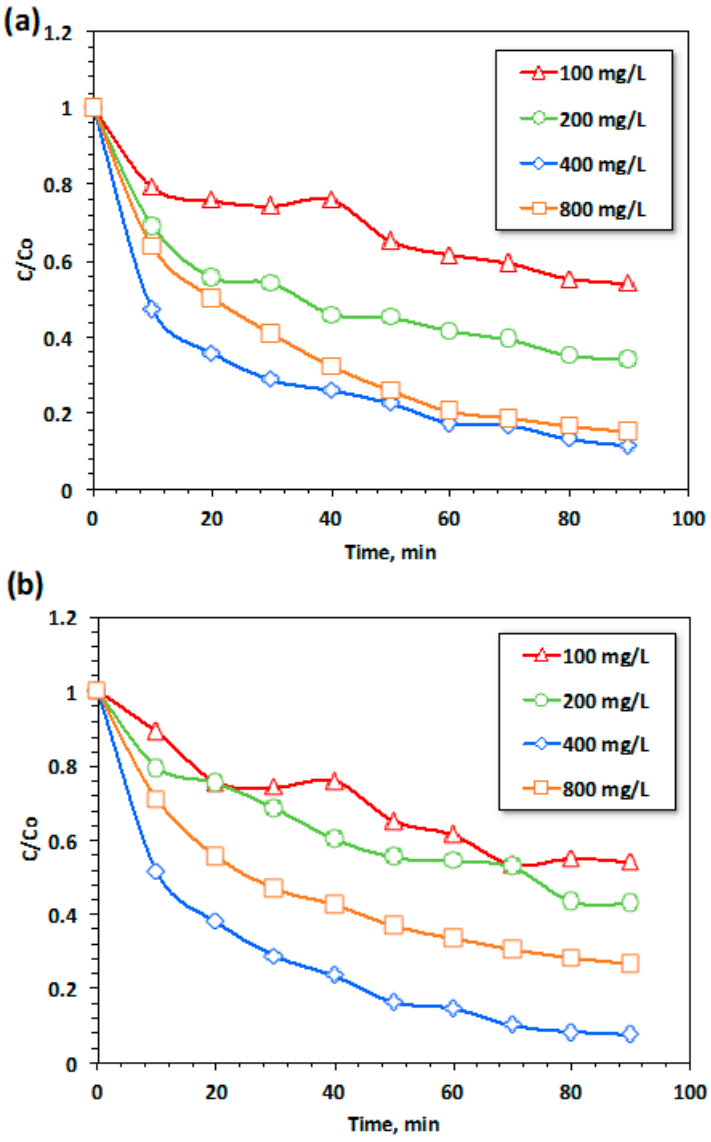

Figure 9. The effect of H_2O_2 concentration on RB4 oxidation at pH 3.0 and catalyst 40 mg/L for (a) ZnO and (b) ZnO-OA based Fenton's systems.

 doi:10.20944/preprints202410.1039.v1

3.2.3.3. Effect of pH

In Fenton's based oxidation system, the aqueous stream pH is signified as a valuable controlled parameter. The influence of initial aqueous solution pH on the oxidation affinity of RB4 dye using silica supported iron Fenton was assessed within the pH range 3.0 to 8.0. The average of the duplicated experimental results of RB4 dye removals are plotted in Figure 10a,b for ZnO and ZnO-OA based Fenton's systems, respectively.

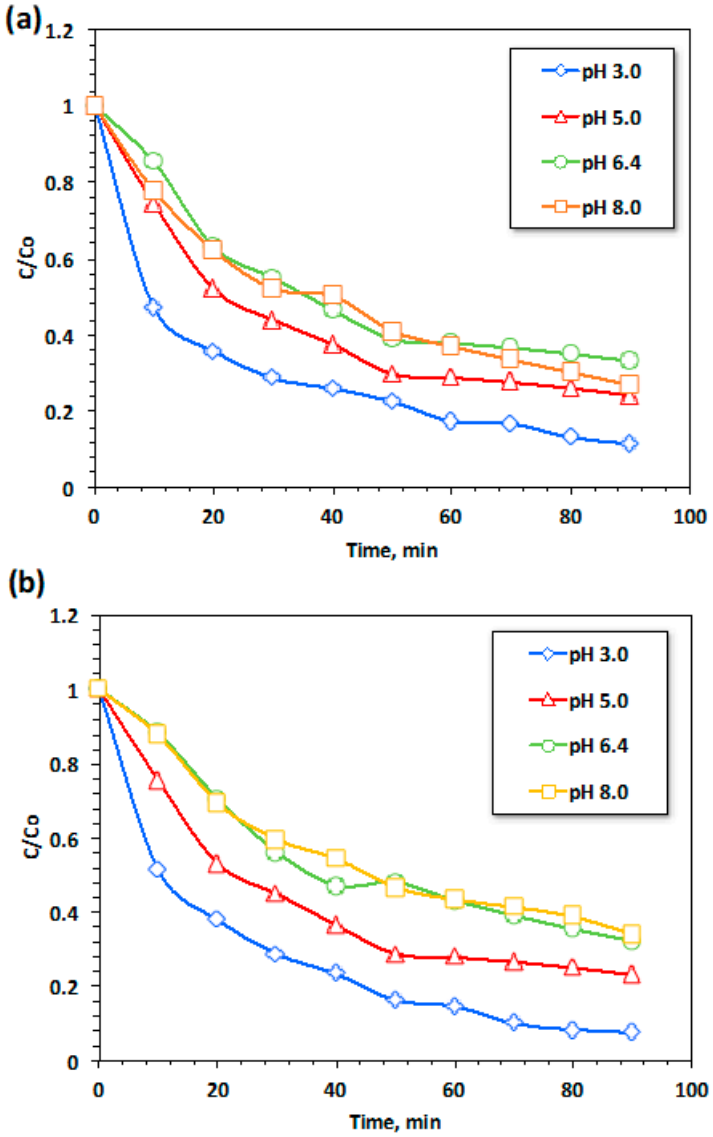

Figure 10. The effect of pH on RB4 oxidation at hydrogen peroxide 400 mg/L and catalyst 40 mg/L for (a) ZnO and (b) ZnO-OA based Fenton's systems.

The data displayed in Figure 10a,b show that pH considerably affected RB4 dye oxidation system, specifically under the acidic pH range (pH 3.0). According to the results exhibited in the curves in Figure 10a, the RB4 dye concentration removal is increased from 66 to 88% as the pH altered from the original pH (6.4) of the solution to the acidic pH (3.0). A similar trend with a higher oxidation efficiency increased from 67 to 93% when the pH is changed to the acidic range for the ZnO-OA based Fenton's systems as seen in Figure 10b. Furthermore, the alkaline pH (8.0) for both systems also reduces oxidation efficiency.

The reason that ZnO based Fenton system behaved differently at different solution pHs could be associated with the production of the •OH radicals. This verifies that both the ZnO speciation and

 doi:10.20944/preprints202410.1039.v1

hydrogen peroxide decomposition are influenced by the pH value. Additionally, the rate of hydroxyl radicals' generation is intensely enhanced at the acidic pH medium. Optimal pH plays an important role in the •OH production. Meanwhile, above or below this limit, reduces the reactive radical's formation. ZnO ions might be generated at high pH values as well as other complexes that might possess low catalytic activity that could also be produced. Additionally, below the optimal pH, more H^+ is generated in the reaction medium, which is further scavenging the •OH radicals' activity. Thereby, it is important to control the pH of the aqueous RB4 dye solution in this narrow acidic range. Previous authors confirmed this phenomenon as the terminal effect of the Fenton's system at pH 3.0 [33–36,51].

3.2.4. Temperature Effects on Kinetics and Thermodynamic Variables

In the photocatalytic oxidation systems, temperature influence is signified as an important parameter that influences the oxidation reaction rates. To assess the effect of temperature on reaction kinetics, RB4 dye oxidation experiments at a temperature ranging from 28 °C to 60 °C were carried out. The results exhibited in Figure 11 illustrate the reduction in RB4 dye oxidation efficiency from 88% to only 74% over the temperature range investigated for the ZnO based system and from 93 to 64% for the ZnO-OA based system. Such a trend might be associated with the hydrogen peroxide reagent that might be thermally decomposed into oxygen and water rather than producing •OH radicals. Additionally, the too high temperature elevation accelerates the presence of ZnO leachate in the medium and the catalyst might be lost. Furthermore, the high temperature could deteriorate the heterogeneous catalyst capped material i.e. OA and thus losing its efficiency. Thus, the rate of deterioration in the dye removal is higher in the ZnO-OA system.

Hence, the overall RB4 dye oxidation rate is a temperature-dependent system. Numerous investigators [29–33] have designated beforehand the experimental evidence for the dependency of catalytic oxidation on temperature. Additionally, previous investigators [38,54] reported that the catalytic oxidation of the Fenton reaction has an optimal temperature, which is a controlling step for such a reaction.

Commonly, Fenton oxidation system is signified as a complex reaction in nature because it involves simultaneous oxidation and adsorption processes. Furthermore, the reaction comprises numerous oxidation species. Thus, the result is a complex reaction and examining its kinetics is also not simple. The models of the zero-, first- and second-order reaction kinetics are applied to assess the reaction kinetics at various temperatures over the studied range.

The corresponding kinetic constants for the zero-, first- and second-order reaction kinetic models, i.e. k_o, k_1 and k_2, respectively, are explored, and the results are tabulated in Table 3. The regression coefficients (R^2) values are exposed to evaluate such models. Consequently, the results from this study listed in Table 3 signify that the system follows second-order kinetics. Additionally, for both systems, the minimal value of half-life time ($t_{1/2}$) corresponds to the 28 ºC reaction temperature. Such examination has been previously stated in similar studies using homogeneous Fenton systems [25,38].

Table 3. Zero-, first- and second-reaction kinetic models rate constants and $t_{1/2}$ of modifies Fenton's system.

T, °C	Zero-order reaction kinetics			First-order reaction kinetics			Second-order reaction kinetics		
	k_0, min^{-1}	R^2	$t_{1/2}$, *min*	k_1, min^{-1}	R^2	$t_{1/2}$, *min*	k_2, L/mg.min	R^2	$t_{1/2}$, *min*
ZnO based Fenton system									
28 °C	0.0036	0.69	45.13	0.0251	0.9	33.804	0.218	0.97	14.11
40 °C	0.0037	0.83	43.91	0.24	0.97	2.783	0.187	0.98	16.45
50 °C	0.0039	0.84	41.66	0.249	0.96	2.88	0.185	0.99	16.63
60 °C	0.0034	0.78	47.79	0.0205	0.92	27.61	0.14	0.99	21.97
ZnO-OA based Fenton system									

 doi:10.20944/preprints202410.1039.v1

28 °C	0.0039	0.77	41.66	0.0304	0.95	38.5	0.3005	0.98	10.23
40 °C	0.0035	0.89	46.42	0.0289	0.98	31.78	0.289	0.97	10.64
50 °C	0.0038	0.9	42.76	0.0218	0.98	23.9	0.1409	0.99	21.83
60 °C	0.0035	0.88	46.42	0.018	0.94	22.79	0.0988	0.97	31.14

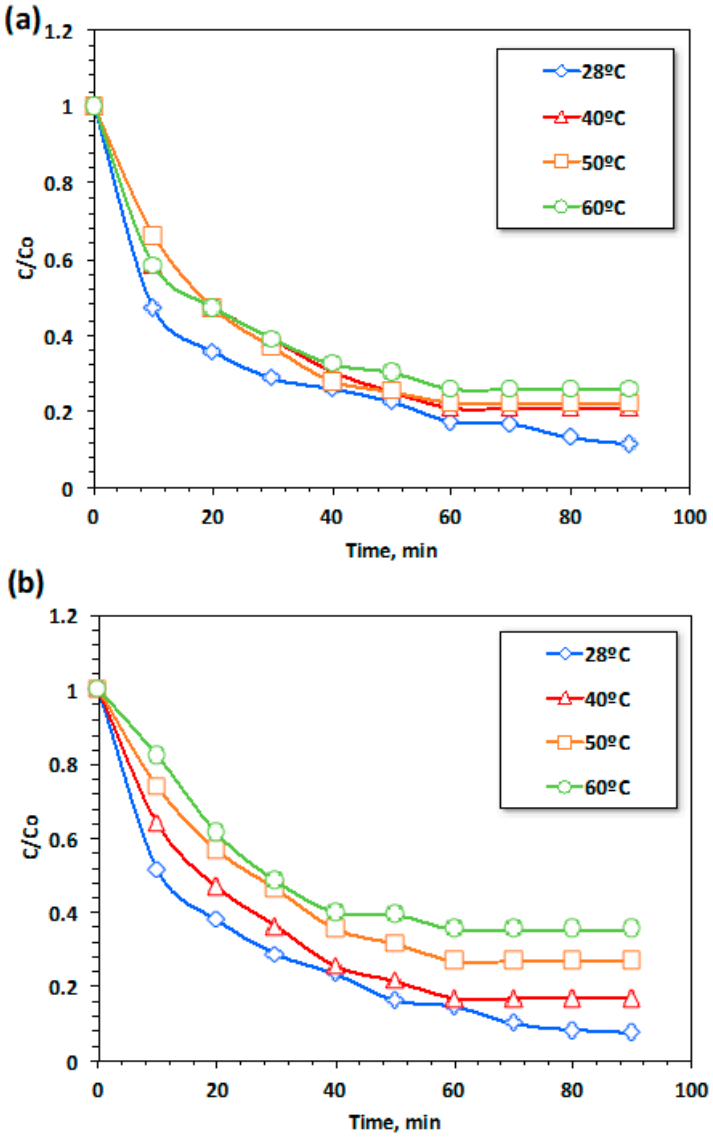

Figure 11. The effect of temperature on RB4 oxidation at pH 3.0, hydrogen peroxide 400 mg/L and catalyst 40 mg/L for (a) ZnO and (b) ZnO-OA based Fenton's systems.

For the object of in-depth understanding the RB4 oxidation system-based Fenton's reaction, the thermodynamic variables are projected. Thermodynamic parameters including the enthalpy of activation (ΔH^{o}), the entropy of activation (ΔS^{o}) and Gibbs free energy of activation (ΔG^{o}) are assessed via using equations (1-4). Moreover, the energy of activation is estimated from the slope of ($-E_a/R$) of the plot in Figure 12.

$$k_2 = Ae^{\frac{-E_a}{RT}} \quad (1)$$

where k_2 is the second order reaction kinetic rate constant (L/mg. min); *Ea* is the activation energy (kJ/mol); R is the universal gas constant (8.314 J/mol·K); T is the temperature (K) and A is the Arrhenius factor [52]. Moreover, Gibbs free energy of activation ($\Delta G°$) was calculated using Eyring's equation [45] according to the following equation:

 doi:10.20944/preprints202410.1039.v1

$$k_2 = \frac{k_B T}{h} e^{(-\frac{\Delta G^\circ}{RT})} \quad (2)$$

where kB is the Boltzmann constant (1.3805 X10^{-23} J/K), and h is Planck's constant (6.6256 X 10^{-34} J s). Furthermore, the enthalpy of activation (ΔH^o) and the entropy of activation (ΔS^o) were evaluated by applying the equations (3) and (4), respectively [45,55].

$$\Delta H^\circ = E_a - RT \quad (3)$$

$$\Delta S^\circ = (\Delta H^\circ - \Delta G^\circ)/T \quad (4)$$

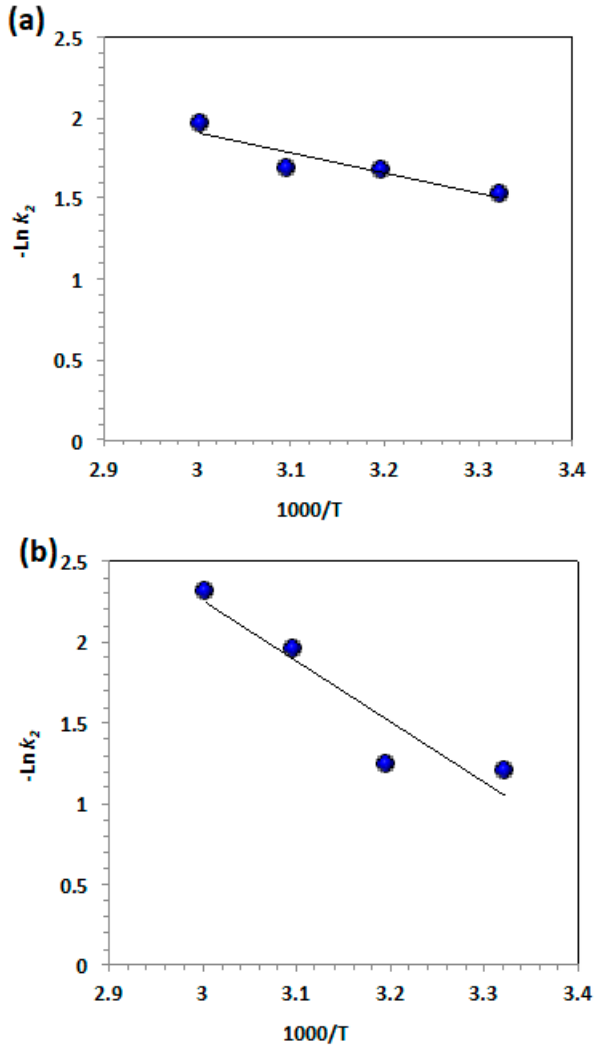

Figure 12. The Arrhenius plot of the second-order kinetic constants for (a) ZnO and (b) ZnO-OA based Fenton's systems.

Subsequently, the thermodynamic variables are assessed according to the above-mentioned equations and the values are tabulated in Table 4. The values of ΔS° for both the ZnO and ZnO-OA based Fenton oxidation are negative but support the reduction of entropy (randomness). Negative ΔS° values suggest the reaction is exothermic in nature. Also, a positive Gibbs free energy value indicates the modified Fenton reaction oxidation process works in a spontaneous nature. Such results have previously concluded in treating wastewater through Fenton's system [38]. Also, the reaction is conducted at a low energy barrier of 10.38 and 31.38 kJ/mol for ZnO-OA and the pristine ZnO based Fenton reaction, respectively.

 doi:10.20944/preprints202410.1039.v1

Table 4. Thermodynamic parameters of ZnO and ZnO-OA based Fenton reaction system.

T, °C	Ln k_1	Ea, kJ/mol	Δ Gº, kJ/mol	ΔHº, kJ/mol	ΔSº, J/mol
ZnO based Fenton system					
28 °C	-1.52	10.38	77.55	7.88	-231.46
40 °C	-1.67		81.15	7.78	-234.38
50 °C	-1.68		83.85	7.70	-235.76
60 °C	-1.96		87.30	7.61	-239.29
ZnO-OA based Fenton system					
28 °C	-1.20	31.38	76.75	28.88	-159.03
40 °C	-1.24		80.01	28.78	-163.68
50 °C	-1.95		84.58	28.69	-173.02
60 °C	-2.31		88.26	28.61	-179.15

4. Conclusion

The synthesis of ZnO nanoparticles was achieved through a thermal decomposition approach. A surface-treated ZnO sample was prepared via an equal proportion of ZnO powder and oleic acid (OA). X-ray diffraction (XRD) results validated the wurtzite structure of the ZnO. The application of OA for surface modification led to a significant enhancement in both the average crystallite sizes and cell volume, An efficient capping of ZnO nanoparticles by OA is obtained leads to improving in the dispersion of the nanoparticle. The modified ZnO and capped ZnO-OA Fenton system displayed an efficient treatment technology for RB4 dye contaminated wastewater using a lab-scale UV illumination photo system. RB4 dye was oxidized with the synthesized ZnO and capped ZnO-OA nanoparticles as a key source of modified Fenton reagent. The maximum oxidation rate, which reached complete removal, is recorded at low dye concentration using 40 and 400 mg/L of ZnO-OA and H_2O_2, respectively, and pH 3.0. Also, capped ZnO-OA showed a pronounced effect comparable to the ZnO-based catalyst. Increasing the temperature from ambient temperature reduces the dye removal rate, which indicates the reaction is exothermic in nature. The kinetic data showed the reaction following the second-order kinetics with minimal global activation energy. Thus, it could be concluded that the process is a promising methodology that could treat RB4 aqueous effluent in a cost-efficient, sustainable approach.

Acknowledgments: 'This work was supported by the Deanship of Scientific Research, Vice Presidency for Graduate Studies and Scientific Research, King Faisal University, Saudi Arabia [Grant No. KFU241974]'.

References

1. Shamberger, P. J.; Bruno, N. M., Review of metallic phase change materials for high heat flux transient thermal management applications. *Applied Energy* **2020**, *258*, 113955.
2. Hu, B.; ai, Y.; Jin, J.; Hayat, T.; Alsaedi, A.; Zhuang, L.; Wang, X., Efficient elimination of organic and inorganic pollutants by biochar and biochar-based materials. *Biochar* **2020,** 2.
3. Chen, Z.; Zhang, S.; Liu, Y.; Alharbi, N.; Rabah, S.; Wang, S.; Wang, X., Synthesis and fabrication of g-C3N4-based materials and their application in elimination of pollutants. *Science of The Total Environment* **2020**, *731*, 139054.
4. Magnago, R.; Berselli, D.; Medeiros, P., Treatment of wastewater from car wash by fenton and photo-fenton oxidative processes. *Journal of Engineering Science and Technology* **2018**, *13*, 838-850.
5. Singh, P.; Sharma, R. K.; Goyal, R.; Hekimoğlu, G.; Sarı, A.; Rathore, P. K. S.; Tyagi, V. V., Development and characterization a novel leakage-proof form stable composite of graphitic carbon nitride and fatty alcohol for thermal energy storage. *Journal of Energy Storage* **2022**, *55*, 105761.
6. Gowthami, D.; Sharma, R. K.; Ansu, A. K.; Sarı, A.; Tyagi, V. V.; Rathore, P. K. S., Evaluation of carbonized cotton stalk for development of novel form stable composite phase change materials for solar thermal energy storage. *Process Safety and Environmental Protection* **2024**, *188*, 1037-1048.
7. Yadav, D. K.; Rathore, P. K. S.; Singh, R. K.; Gupta, A. K.; Sikarwar, B. S., Experimental Study on Paraffin Wax and Soya Wax Supported by High-Density Polyethylene and Loaded with Nano-Additives for Thermal Energy Storage. *Energies* **2024**, *17*, 2461.

8. Poormand, H.; Leili, M.; Khazaei, M., Adsorption of methylene blue from aqueous solutions using water treatment sludge modified with sodium alginate as a low cost adsorbent. *Water Science and Technology* **2016,** 75.
9. Saleem, M.; Liang, F.; Ruan, H.; Wu, F.; Huang, Q.; Xu, C. L.; Kong, C., Effect of zinc acetate concentration on the structural and optical properties of ZnO thin films deposited by Sol-Gel method. *Int. J. Phys. Sci.* **2012,** 7.
10. Srivastava, V. C.; Swamy, M. M.; Mall, I. D.; Prasad, B.; Mishra, I. M., Adsorptive removal of phenol by bagasse fly ash and activated carbon: Equilibrium, kinetics and thermodynamics. *Colloids and Surfaces A: Physicochemical and Engineering Aspects* **2006**, *272*, 89-104.
11. Markandeya, n.; Shukla Sheo, P.; Dhiman, N.; Mohan, D.; Kisku Ganesh, C.; Roy, S., An Efficient Removal of Disperse Dye from Wastewater Using Zeolite Synthesized from Cenospheres. *Journal of Hazardous, Toxic, and Radioactive Waste* **2017**, *21*, 04017017.
12. Elsayed, S. A.; El-Sayed, I. E. T.; Tony, M. A., Impregnated chitin biopolymer with magnetic nanoparticles to immobilize dye from aqueous media as a simple, rapid and efficient composite photocatalyst. *Applied Water Science* **2022**, *12*, 252.
13. Sekhula, M.; Okonkwo, O.; Zvinowanda, C., Fixed bed column adsorption of Cu(II) onto maize Tassel-PVA beads. *Journal of Chemical Engineering & Process Technology* **2012,** 03.
14. Deng, D.; Lin, O.; Rubenstein, A.; Weidhaas, J.; Lin, L.-S., Elucidating biochemical transformations of Fe and S in an innovative Fe(II)-dosed anaerobic wastewater treatment process using spectroscopic and phylogenetic analyses. *The Chemical Engineering Journal* **2019**, *358*, 1208-1217.
15. Argun, M. E.; Karatas, M., Application of Fenton process for decolorization of reactive black 5 from synthetic wastewater: Kinetics and thermodynamics. *Environmental Progress & Sustainable Energy* **2011**, *30*, 540-548.
16. Dubber, D.; Gray, N., Replacement of chemical oxygen demand (COD) with total organic carbon (TOC) for monitoring wastewater treatment performance to minimize disposal of toxic analytical waste. *Journal of environmental science and health. Part A, Toxic/hazardous substances & environmental engineering* **2010**, *45*, 1595-600.
17. Aziz, J. A.; Tebbutt, T. H. Y., Significance of COD, BOD and TOC correlations in kinetic models of biological oxidation. *Water Research* **1980**, *14*, 319-324.
18. Pintor, A. M. A.; Vilar, V. J. P.; Boaventura, R. A. R., Decontamination of cork wastewaters by solar-photo-Fenton process using cork bleaching wastewater as H2O2 source. *Solar Energy* **2011**, *85*, 579-587.
19. Ioannou, L. A.; Fatta-Kassinos, D., Solar photo-Fenton oxidation against the bioresistant fractions of winery wastewater. *Journal of Environmental Chemical Engineering* **2013**, *1*, 703-712.
20. Bounab, L.; Iglesias, O.; González-Romero, E.; Pazos, M.; Ángeles Sanromán, M., Effective heterogeneous electro-Fenton process of m-cresol with iron loaded actived carbon. *RSC Advances* **2015**, *5*, 31049-31056.
21. Buthiyappan, A.; Abdul Raman, A. A.; Daud, W. M. A. W., Development of an advanced chemical oxidation wastewater treatment system for the batik industry in Malaysia. *RSC Advances* **2016**, *6*, 25222-25241.
22. Bautista, P.; Mohedano, A. F.; Casas, J. A.; Zazo, J. A.; Rodriguez, J. J., An overview of the application of Fenton oxidation to industrial wastewaters treatment. *Journal of Chemical Technology & Biotechnology* **2008**, *83*, 1323-1338.
23. Xu, H.; Li, M.; Wang, H.; Miao, J.; Zou, L., Fenton Reagent Oxidation and Decolorizing Reaction Kinetics of Reactive Red SBE. *Energy Procedia* **2012**, *16*, 58-64.
24. Jefferson, B.; Palmer, A.; Jeffrey, P.; Stuetz, R.; Judd, S., Grey water characterisation and its impact on the selection and operation of technologies for urban reuse. *Water Science and Technology* **2004**, *50*, 157-164.
25. Ji, F.; Li, C.; Zhang, J.; Deng, L., Efficient decolorization of dye pollutants with LiFe(WO4)2 as a reusable heterogeneous Fenton-like catalyst. *Desalination* **2011**, *269*, 284-290.
26. Bradu, C.; Frunza, L.; Mihalche, N.; Avramescu, S.-M.; Neaţă, M.; Udrea, I., Removal of Reactive Black 5 azo dye from aqueous solutions by catalytic oxidation using CuO/Al2O3 and NiO/Al2O3. *Applied Catalysis B: Environmental* **2010**, *96*, 548-556.
27. Kumar, S. G.; Devi, L. G., Review on Modified TiO2 Photocatalysis under UV/Visible Light: Selected Results and Related Mechanisms on Interfacial Charge Carrier Transfer Dynamics. *The Journal of Physical Chemistry A* **2011**, *115*, 13211-13241.
28. Zaneti, R. N.; Etchepare, R.; Rubio, J., Car wash wastewater treatment and water reuse – a case study. *Water Science and Technology* **2013**, *67*, 82-88.
29. Bwapwa, J. K.; Jaiyeola, A. T.; Chetty, R., Bioremediation of acid mine drainage using algae strains: A review. *South African Journal of Chemical Engineering* **2017**, *24*, 62-70.
30. Deng, D.; Lin, L.-S., Continuous sulfidogenic wastewater treatment with iron sulfide sludge oxidation and recycle. *Water Research* **2017**, *114*, 210-217.

31. Villegas-Guzman, P.; Giannakis, S.; Rtimi, S.; Grandjean, D.; Bensimon, M.; de Alencastro, L.; Torres-Palma, R.; Pulgarin, C., A green solar photo-Fenton process for the elimination of bacteria and micropollutants in municipal wastewater treatment using mineral iron and natural organic acids. *Applied Catalysis B Environmental* **2017**, *219*, 538-549.
32. Fang, H.; Zhang, H.; Han, L.; Mei, J.; Ge, Q.; Long, Z.; Yu, Y., Exploring bacterial communities and biodegradation genes in activated sludge from pesticide wastewater treatment plants via metagenomic analysis. *Environmental Pollution* **2018**, *243*, 1206-1216.
33. Singh, A. K.; Srivastava, O. N.; Singh, K., Shape and Size-Dependent Magnetic Properties of Fe3O4 Nanoparticles Synthesized Using Piperidine. *Nanoscale Research Letters* **2017**, *12*, 298.
34. Ali, F.; Khan, S. B.; Kamal, T.; Alamry, K. A.; Asiri, A. M.; Sobahi, T. R. A., Chitosan coated cotton cloth supported zero-valent nanoparticles: Simple but economically viable, efficient and easily retrievable catalysts. *Scientific Reports* **2017**, *7*, 16957.
35. Joshi, S.; Garg, V. K.; Kataria, N.; Kadirvelu, K., Applications of Fe3O4@AC nanoparticles for dye removal from simulated wastewater. *Chemosphere* **2019**, *236*, 124280.
36. Liu, L.; Liu, S.; Mishra, S. B.; Sheng, L., An easily applicable and recyclable Fenton-like catalyst produced without wastewater emission and its performance evaluation. *Journal of Cleaner Production* **2019**, *234*, 653-659.
37. Barnasas, A.; Karavasilis, M. V.; Aggelopoulos, C.; Poulopoulos, P., Growth and Characterization of Nanostructured Ag-ZnO for Application in Water Purification. *Trans Tech Publications* **2020**, *62*, 75-86.
38. Farha, A. H.; Al Naim, A. F.; Mansour, S. A., Cost-Effective and Efficient Cool Nanopigments Based on Oleic-Acid-Surface-Modified ZnO Nanostructured. *Materials* **2023**, *16*, 2159.
39. Lin, C.-C.; Li, Y.-Y., Synthesis of ZnO nanowires by thermal decomposition of zinc acetate dihydrate. *Materials Chemistry and Physics* **2009**, *113*, 334-337.
40. Alkallas, F. H.; Elshokrofy, K. M.; Mansour, S. A., Structural and Diffuse Reflectance Study of Cr-Doped ZnO Nanorod-Pigments Prepared via Facile Thermal Decomposition Technique. *Journal of Inorganic and Organometallic Polymers and Materials* **2019**, *29*, 792-798.
41. Liu, P.; Su, Z., Preparation and Characterization of PMMA/ZnO Nanocomposites via In‐Situ Polymerization Method. *Journal of Macromolecular Science, Part B* **2006**, *45*, 131-138.
42. Mansour, S. A.; Farha, A. H.; Tahoun, B. A.; Elsad, R. A., Novel magnetic polyaniline nanocomposites based on as-synthesized and surface modified Co-doped ZnO diluted magnetic oxide (DMO) nanoparticles. *Materials Science and Engineering: B* **2021**, *265*, 115032.
43. Mote, V.; Purushotham, Y.; Dole, B., Williamson-Hall analysis in estimation of lattice strain in nanometer-sized ZnO particles. *Journal of Theoretical and Applied Physics* **2012,** 6.
44. Hong, R.; Pan, T.; Qian, J.; Li, H., Synthesis and surface modification of ZnO nanoparticles. *Chemical Engineering Journal* **2006**, *119*, 71-81.
45. Tony, M. A.; Mansour, S. A., Synthesis of nanosized amorphous and nanocrystalline TiO2 for photochemical oxidation of methomyl insecticide in aqueous media. *Water and Environment Journal* **2020,** 34, (S1), 239-249.
46. Zhao, Y. Q.; Keogh, C.; Tony, M. A., On the necessity of sludge conditioning with non-organic polymer: AOP approach. *Journal of Residuals Science & Technology* **2009**, *6*, 151-155.
47. Tony, M. A.; Lin, L.-S., Iron Coated-Sand from Acid Mine Drainage Waste for Being a Catalytic Oxidant Towards Municipal Wastewater Remediation. *International Journal of Environmental Research* **2021**, 1-11.
48. Tony, M. A.; Purcell, P. J.; Zhao, Y.; Tayeb, A. M.; El-Sherbiny, M. F., Kinetic modeling of diesel oil wastewater degradation using photo-Fenton process. *Environmental Engineering & Management Journal (EEMJ)* **2015,** 14, (1).
49. Hu, X.; Wang, X.; Ban, Y.; Ren, B., A comparative study of UV–Fenton, UV–H2O2 and Fenton reaction treatment of landfill leachate. *Environmental technology* **2011**, *32*, 945-951.
50. Primo, O.; Rueda, A.; Rivero, M. J.; Ortiz, I., An integrated process, Fenton reaction− ultrafiltration, for the treatment of landfill leachate: pilot plant operation and analysis. *Industrial & engineering chemistry research* **2008**, *47*, 946-952.
51. Hamd, W.; Dutta, J., Heterogeneous photo-Fenton reaction and its enhancement upon addition of chelating agents. 2020; pp 303-330.
52. Abdollahzadeh, H.; Fazlzadeh, M.; Afshin, S.; Arfaeinia, H.; Feizizadeh, A.; Poureshgh, Y.; Rashtbari, Y., Efficiency of activated carbon prepared from scrap tires magnetized by Fe3O4 nanoparticles: characterisation and its application for removal of reactive blue19 from aquatic solutions. *International Journal of Environmental Analytical Chemistry* **2022**, *102*, 1911-1925.
53. Tony, M. A.; Ali, I. A., Mechanistic implications of redox cycles solar reactions of recyclable layered double hydroxides nanoparticles for remazol brilliant abatement. *International Journal of Environmental Science and Technology* **2022**, *19*, 9843-9860.

 doi:10.20944/preprints202410.1039.v1

54. Najjar, W.; Chirchi, L.; Santos, E.; Ghorhel*, A., Kinetic study of 2-nitrophenol photodegradation on Al-pillared montmorillonite doped with copper. *Journal of Environmental Monitoring* **2001**, *3*, 697-701.
55. Tony, M. A.; Lin, L.-S., Performance of acid mine drainage sludge as an innovative catalytic oxidation source for treating vehicle-washing wastewater. *Journal of Dispersion Science and Technology* **2021**, *43*, 50-60.